Temperature Inversion Breakup with Impacts on Air Quality in Urban Valleys Influenced by Topographic Shading

ANGELA M. RENDÓN, JUAN F. SALAZAR, AND CARLOS A. PALACIO

El Grupo de Ingeniería y Gestión Ambiental, Escuela Ambiental, Facultad de Ingeniería, Universidad de Antioquia, Medellín, Colombia

VOLKMAR WIRTH

Institute for Atmospheric Physics, Johannes Gutenberg University Mainz, Mainz, Germany

(Manuscript received 8 May 2014, in final form 27 September 2014)

ABSTRACT

Urban valleys can experience serious air pollution problems as a combined result of their limited ventilation and the high emission of pollutants from the urban areas. Idealized simulations were analyzed to elucidate the breakup of an inversion layer in urban valleys subject to a strong low-level temperature inversion and topographic effects on surface heating such as topographic shading, as well as the associated air pollution transport mechanisms. The results indicate that the presence and evolution in time of the inversion layer and its interplay with an urban heat island within the valley strongly influence the venting of pollutants out of urban valleys. Three mechanisms of air pollution transport were identified. These are transport by upslope winds, transport by an urban heat island–induced circulation, and transport within a closed slope-flow circulation below an inversion layer.

1. Introduction

Urban valleys can experience serious air pollution problems as a combined result of their limited ventilation and the high emission of pollutants from the urban areas (e.g., Rutllant and Garreaud 1995; Malek et al. 2006; Chu et al. 2008). In such complex terrains, the venting of pollution out of the valley is limited by the topography and can be further restricted by local circulations (Gohm et al. 2009), and particularly by urban heat island–induced circulations (Haeger-Eugensson and Holmer 1999; Savijärvi and Liya 2001) and low-level temperature inversions (Janhall et al. 2006; Yao and Zhong 2009; Rendón et al. 2014). The occurrence of inversion layers near the ground, that is layers where the potential temperature increases with height (Whiteman 1982), are common in urban areas and mountain valleys (Oke 1995; Whiteman 2000).

The destruction of an inversion layer is termed the breakup of the temperature inversion (BTI). This process can have a large influence on the air quality of urban areas in complex terrain. Different studies confirm the association between the occurrence and persistence of temperature inversions and the presence of high concentrations of air pollutants in urban valleys. For instance, heavy air pollution events experienced in the city of Santiago in the Central Valley in Chile (Rutllant and Garreaud 1995), the city of Logan in the Cache Valley of Utah in the United States (Malek et al. 2006), and the Lanzhou urban valley in China (Chu et al. 2008) have been associated with low-level inversions.

In a valley, inversions are destroyed by the combined effects of two processes: the upward growth of a convective boundary layer (CBL) from the ground, and the removal of air from the base of the inversion by the upslope flows that develop over heated sidewalls, which in turn induces subsidence warming over the valley center (Whiteman and McKee 1982; Whiteman 1982; Zoumakis and Efstathiou 2006). Both processes are driven by the heating of the surface, which produces thermal winds and turbulence.

The heating of the surface in an urban valley can have large spatial variations due to the presence of an urban heat island (UHI), and it exhibits a diurnal cycle that is

Corresponding author address: Angela M. Rendón, Universidad de Antioquia, Calle 70 No. 52-21, of. 20-414, Medellín, Colombia.
E-mail: angela.rendon@udea.edu.co

DOI: 10.1175/JAMC-D-14-0111.1

largely influenced by the spatial and temporal variations of the solar radiation that reaches the ground. The orientation of the valley sidewalls with respect to the sun can force asymmetric irradiation conditions owing to topographic effects such as topographic shading (Matzinger et al. 2003; Hoch and Whiteman 2010) and because the absorption of solar radiation depends on the inclination of the surface (Hay and McKay 1985; Whiteman et al. 1989). Both modeling and observational studies have noted several implications of this asymmetry on the slope and valley wind system, as well as the associated impacts on the inversion dynamics and the venting of pollution. The topographic shading can delay the BTI and lead to an asymmetric development of the CBL along the valley floor and slopes (Anquetin et al. 1998; Colette et al. 2003). Such a delay can have significant impacts on air quality (Rendón et al. 2014), mainly because the presence of an inversion layer tends to reduce the mass flux in the slope wind layer (Vergeiner and Dreiseitl 1987). Asymmetric thermal forcing of the valley sidewalls may result in an asymmetry in wind circulation and air pollutants distribution (Gohm et al. 2009; Lehner and Gohm 2010), as well as in the development of cross-valley flows (Lehner and Gohm 2010). Pollutants in the slope flow may remain trapped in a closed slope-flow circulation (Reuten et al. 2005), which has been described in some studies as a "smog trap" situation. This smog trap can be enhanced by UHI-induced circulations (Savijärvi and Liya 2001; Rendón et al. 2014).

The present paper follows up our previous study about the effects of urbanization on the BTI and the accompanying impacts on air quality (Rendón et al. 2014). Here we investigate the influence that the orientation of an urban valley subject to a strong temperature inversion has on its local atmospheric dynamics and pollution, owing to the topographic effects on surface heating. In particular, we examine the evolution in time of the BTI and the associated mechanisms of air pollution transport, through idealized simulations performed with the Eulerian/Lagrangian (EULAG) numerical model (Prusa et al. 2008). The simulations are idealized in the sense that they are conducted with idealized topography, surface heating, and some atmospheric conditions including the absence of moisture and the structure of the initial inversion layer (further details are given in section 2). The remainder of the paper is organized as follows: the model and the experiment are described in section 2, results are presented in section 3 and discussed in section 4, and the conclusions are drawn in section 5.

2. Model description and experiment design

The model setup is the same of our previous study (Rendón et al. 2014), but with two differences. First, the model now includes an algorithm for representing the influence of the topographic shading and the dependence of the solar radiation absorption on the inclination of the surface (Bellasio et al. 2005). Second, in the present study the topography is different, the valleys are deeper, and their sidewalls are steeper, as compared with the valleys studied in Rendón et al. (2014). Our idealized approach is similar to that of other previous studies about thermal winds in valleys (e.g., Anquetin et al. 1998; Colette et al. 2003; Serafin and Zardi 2010a; Schmidli et al. 2011). Further details about the model (section 2a), the experiment (section 2b), and the model setup (section 2c) are given below.

a. Model description

The numerical model adopted in this study is EULAG, which has been thoroughly documented in the literature (Prusa et al. 2008, and references therein), and has been applied to investigate the daytime evolution of the thermal wind circulation in valleys (Schmidli et al. 2011; Rendón et al. 2014), among other topics generally related to fluid dynamics of compressible or incompressible fluids.

In the present study EULAG was configured as a nonhydrostatic model that solves the anelastic equations of motion in terrain-following coordinates, under the Ogura and Phillips (1962) approximation of the atmosphere. The model employs an explicit predictive equation for turbulent kinetic energy (TKE) and uses a local Deardorff-type TKE closure derived for large-eddy simulations for which the length scale is based on the grid spacing (Deardorff 1980). Surface drag is accounted for through the usual bulk formula with a drag coefficient $C_D = 0.01$. We modified the EULAG code to account for the topographic shading and the effects of solar radiation on the heating of inclined surfaces according to the algorithm of Bellasio et al. (2005). Further details about this are given below.

b. Experiment design

The basic idea of the model experiment consists in comparing the BTI and the transport of air pollutants in two distinctly oriented urban valleys. Both valleys are the same but for their geographic orientation: one valley is oriented south–north (S–N valley), while the other is oriented east–west (E–W valley). Our experiment can be viewed as a numerical development of the conceptual experiment proposed by Lehner et al. (2011; see their Fig. 1). In a simple south–north-oriented valley, as the sun rises in the morning, the east-facing slope can receive direct radiation while the west-facing slope is still shaded. The opposite situation occurs in the afternoon. This asymmetric irradiation of the valley sidewalls has

implications on dynamics and air pollution (see references in section 1).

For convenience, we will refer to the sidewalls of both valleys as the left and right sidewalls. In the S–N valley "left and right" is equivalent to "west and east," while in the E–W valley it is equivalent to "south and north." We assumed that our valleys are located at the equator (0° latitude). The date chosen is the vernal equinox (yearday 81), when the sun rises directly to the east, sets directly to the west, and, at the equator, follows an east–west path through the sky, with maximum insolation at solar noon. It implies that the path of the sun is either normal or tangential to the cross section of the S–N valley or the E–W valley, respectively.

Each valley has two types of homogeneous land cover: urban and rural, which are distinguished by assuming that the surface heating is higher in the urban areas owing to the thermal properties and impermeability of urban surfaces like concrete or asphalt (Offerle et al. 2006; Nadeau et al. 2009). In both cases, the urban area grows symmetrically from the center of the valley and extends to the lower part of the sidewalls. Although the reported results do not consider the effects of roughness, we tested the sensitivity of our results to the inclusion of these effects under the assumption that the urban areas are rougher than the rural ones, and we found no significant differences. In these test runs the drag coefficient was 0.010 for the urban land and 0.001 for the rural one. A similar sensitivity analysis, with similar results, was made in our previous study (Rendón et al. 2014). All the simulations were performed during the daytime between 0600 and 1800 local standard time (LST), starting with a condition of temperature inversion.

The idealized diurnal cycle of the sensible heat flux was defined through the function

$$Q_h(x,t) = Q_r(x)K(x,t), \tag{1}$$

where $Q_h(x, t)$ is the time- and space-varying flux of sensible heat ($\mathrm{J\,m^{-2}s^{-1}}$), $Q_r(x)$ is a maximum reference value depending on whether the surface at x (x is the horizontal coordinate across the section of the valley) is urban [$Q_r(x) = 300\,\mathrm{J\,m^{-2}s^{-1}}$] or rural [$Q_r(x) = 90\,\mathrm{J\,m^{-2}s^{-1}}$], and $K(x, t)$ is a factor that ranges from 0 to 1 and determines the shape of the diurnal cycle of surface heating. To distinguish both valleys for their geographic orientation, we defined $K(x, t)$ as a function of the radiation that reaches the surface and computed it as

$$K(x,t) = \frac{R_{\mathrm{dif}}(x,t) + R_{\mathrm{ref}}(x,t) + R_{\mathrm{dir}}(x,t)}{R_{\max}}, \tag{2}$$

where $R_{\mathrm{dif}}(x, t)$, $R_{\mathrm{ref}}(x, t)$, and $R_{\mathrm{dir}}(x, t)$ are, respectively, the diffuse, the reflected, and the direct radiation reaching the surface at every location (x) and time (t); $R_{\max}$ is the maximum of all of the values of the sum $R_{\mathrm{dif}}(x, t) + R_{\mathrm{ref}}(x, t) + R_{\mathrm{dir}}(x, t)$, which is included to make $K(x, t)$ dimensionless. These solar radiation components were estimated according to the algorithm of Bellasio et al. (2005), which allows us to consider the spatial variation of the terrain slope and aspect and of the sky view factor, the time variation of the horizon angle and the solar zenith at every location, and the change in radiation depending on the inclination of the surface. These factors are important in controlling the spatial variability of the surface radiation budget in mountainous terrain (Oliphant et al. 2003). It turns out that, for instance, at a given time some points at the valley surface do not receive direct radiation because of topographic shading, which in turn means a reduction in $K(x, t)$ and then in $Q_h(x, t)$. There is no dependence of $Q_h(x, t)$ on y (y is the horizontal coordinate normal to the cross section of the valley) because of the symmetry and orientation of the valleys. Further details about the topography and the coordinate system are given in section 2c(1).

Figure 1 shows the values of $K(x, t)$ for both valleys, and the differences between them. The greater differences are concentrated over the sidewalls with peak values (~0.15) occurring at some points in the midpart of the right sidewall in the morning and in the midpart of the left sidewall in the afternoon. These peak values are associated with the effect of the topographic shading in restricting the direct radiation, which is more pronounced in the right (left) sidewall during the morning (afternoon), in the S–N valley. In the right sidewall, the differences are negative during the morning while slightly positive during the afternoon, which means that in the morning (afternoon) this sidewall is less (more) heated in the S–N valley than in the E–W valley. Analogously, on the left sidewall the differences are negative (positive) during the afternoon (morning). The heating of the sidewalls of the S–N valley is asymmetric, while it is symmetric in the E–W valley.

Equation (1) involves the assumption that the shape of the diurnal cycle of sensible heat is similar to that of net solar radiation, which is in reasonable agreement with previous studies of the surface energy balance (see, e.g., Grimmond and Oke 2002; Matzinger et al. 2003). The values computed through Eq. (1) are on the same order of magnitude as those reported in literature for different urban and rural areas (e.g., Wesson et al. 2001; Grimmond and Oke 2002; Jung et al. 2011). We acknowledge that the representation of surface heating through the described formulation is still very simplified with respect to, for instance, a model of the urban energy balance (e.g., Grimmond and Oke 2002), but it

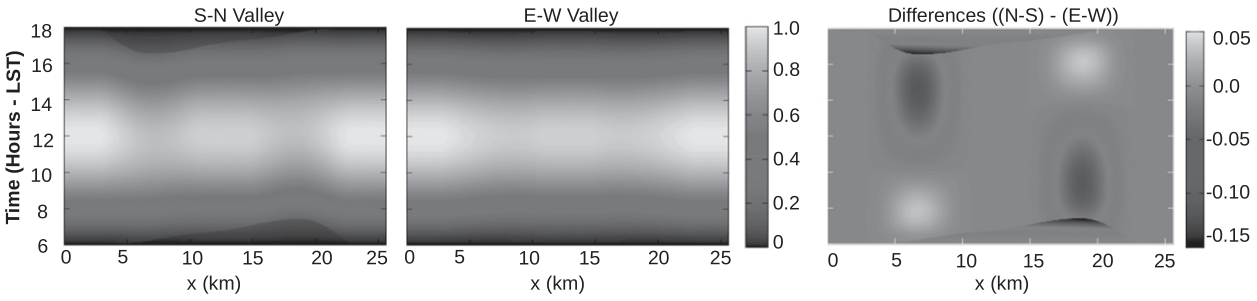

FIG. 1. Dimensionless factor $K(x, t)$ that determines the shape of the diurnal cycle of surface heating depending on the orientation of the valleys and the accompanying topographic effects on solar radiation in the (left) S–N and (center) E–W valleys, and (right) differences of $K(x, t)$ between both valleys.

reasonably represents the main features of the topographic effects that we are studying in an idealized framework.

Urban areas are important sources of air pollution because of factors such as the emission of gases by the industrial (Rosenzweig et al. 2010) or transport sectors (Colvile et al. 2001). To obtain insights into the air quality impacts, we simulate the transport of a passive tracer released from the urban area by assuming that this area acts as a uniform and continuous source, that is, that there is no spatial or temporal heterogeneity of emissions.

It is important to bear in mind that we are not considering any spatial heterogeneity such as that caused by intraurban variations of pollution (Wilson et al. 2005) and surface energy fluxes (Offerle et al. 2006), which are still very complex issues that are strongly dependent on the particularities of each city. Therefore, we regard our assumption of intraurban homogeneity as the simplest possibility, although other assumptions may be raised as well. Neither chemical reactions nor the radiative effects of pollutants in the atmosphere are considered, and we do not include moisture in our simulations at this stage. The presence of moisture will play a complex role in conditioning the efficiency of the valley heating process, causing the release of latent heat but also reducing the radiant energy flux if condensation occurs (Schmidli et al. 2011; Serafin and Zardi 2010a). Future investigations are needed to clarify these issues.

c. Model setup

1) TOPOGRAPHY AND SIMULATION DOMAIN

The domain of the simulations is 25 600 m in the x direction (horizontal coordinate across the valley), 6400 m in the y direction (horizontal coordinate along the valley), and 6400 m in the z direction (vertical coordinate). The horizontal grid is uniform and has a resolution of 50 m, and the vertical grid is set with terrain-following coordinates stretched with a minimum gridcell size of 25 m at the surface and a maximum gridcell size of 121 m at the top of the simulation domain. Although idealized, the topography is loosely based in a reference urban valley, the Aburrá valley in the Colombian Andes, where urbanization has been progressing rapidly and the urban area (Medellín city and its neighboring cities) has expanded beyond the valley floor toward the sidewalls, and it is represented by the function (Rampanelli et al. 2004)

$$z(x) = h\begin{cases} 1, & |x - x_0| > s_x + v_x \\ \dfrac{1}{2}\left[1 - \cos\left(\dfrac{\pi|x - x_0| - v_x}{s_x}\right)\right], & v_x < |x - x_0| < s_x + v_x, \\ 0, & |x - x_0| < v_x \end{cases} \tag{3}$$

where $z(x)$ is the height of the terrain above the valley floor (m), h is the maximum depth of the valley ($h = 2000$ m), x_0 is the x coordinate of the center of the valley ($x_0 = 12\,800$ m), s_x is the width of the sidewalls ($s_x = 8000$ m), and v_x is the half-width of the valley floor ($v_x = 2000$ m). Equation (3) represents a symmetrical cross section, constant along the y direction. In addition, two 2800-m-length plateaus are included in the modeling domain to have the lateral boundaries far from the top of the sidewalls. The average steepness of the sidewalls is 25%, and the transitions between them and the plateaus and the valley floor are smooth to prevent abrupt changes in wind direction.

2) INITIAL AND BOUNDARY CONDITIONS

The initial condition of the simulations is characterized by the presence of a strong low-level temperature inversion and an atmosphere at rest. At the beginning of the simulations (0600 LST), there is an inversion layer in the lowest 800 m above the whole valley floor with a vertical potential temperature gradient ($\partial\theta/\partial z$) of $11\,\mathrm{K\,km^{-1}}$, corresponding to a Brunt–Väisälä frequency of $N^2 = 0.019\,\mathrm{s^{-1}}$. Above the top of the inversion we assume neutral stratification, that is, $\partial\theta/\partial z = 0$ for $z > 800$ m.

The influence of synoptic winds is neglected by defining all the lateral boundaries as periodic. To avoid unrealistic reflection of upward-propagating internal gravity waves aloft, a Rayleigh damping layer of 2000 m is included below the top of the domain (Warner 2011). The bottom and the top of the domain are treated as impermeable boundaries.

3. Results

The different orientation of the valleys leads to differences in the diurnal cycle of the surface heating (Fig. 1) due to the asymmetric irradiation of the sidewalls in the S–N valley where the east-facing (west facing) slope is more heated during the morning (afternoon). The implications of these asymmetries on the evolution in time of the temperature inversion (section 3a), the cross-valley wind system and turbulence (section 3b), and the tracer distribution and transport (section 3c) are examined below. The fields of differences between both valleys presented in several figures are always computed as the values in the S–N valley minus the corresponding values in the E–W valley. All of the results are averaged along the valley (the y direction) to focus our analyses on the dynamics in the valley cross section (the $x-z$ plane). This averaging procedure does not affect the qualitative behavior of the results with respect to a single cross section in the center of the valley. Since the valley has no variation in width along its axis (the y direction), the cross-valley circulation induced by the slope flow can essentially be considered two-dimensional in the cross-valley plane (the $x-z$ plane) (Rampanelli et al. 2004). The plots do not show the entire simulation domain but only the selected region of interest. Recall that a comparison between the left (right) sidewalls of both valleys will be a comparison between the west (east) sidewall of the S–N valley and the south (north) sidewall of the E–W valley.

a. Potential temperature and inversion breakup

Most of the time the core of the S–N valley, including the lower part of the sidewalls, is slightly colder (the maximum difference is ~2.8 K), as indicated by the negative differences shown in Fig. 2. In the early morning (0700 LST; Fig. 2a) the situation is still close to the initial conditions; however, some negative differences slightly skewed toward the right side are found on the valley floor. In the late afternoon (1700 LST; Fig. 2f), the differences are concentrated over the left sidewall, which is colder in the S–N valley because it receives less solar radiation.

The evolution in time of the inversion profiles in the center and along the sidewalls does not show marked differences between the two valleys (Fig. 3). In both valleys the height of the top of the inversion remains substantially unchanged during the BTI, while the base of the inversion is continuously raised until the breakup, which occurs between 1400 and 1500 LST. As will be confirmed in the next section, the development of the CBL over the valley floor is the process that dominates the BTI in both valleys; that is, the breakup is mainly caused by the rise of the bottom of the inversion layer resulting from the growth of the CBL. This BTI pattern can be described as pattern 1 according to the classification proposed by Whiteman (1982) and Whiteman and McKee (1982). In contrast to the previous result that the BTI pattern can change as a result of the expansion of the urban area (Rendón et al. 2014), our present results do not show a significant dependence of the BTI pattern on the topographic shading.

On average, the inversion profiles both in the center of the valley and along the sidewalls are colder in the S–N valley throughout the daytime (Fig. 4). The differences are more marked in the lower part of the right (left) sidewall during the morning (afternoon), that is, where direct radiation is more restricted in the S–N valley (Fig. 1). The transport of heat by the slope winds and the thermal turbulence over the slopes lead to higher variability of θ along the sidewalls than in the center of the valleys (Figs. 3 and 4).

Our results (including plots every 15 min, not shown) do not show a delay in the breakup time as a consequence of the topographic shading. In both valleys, the breakup occurs around 1430 LST. A previous study by Colette et al. (2003) found that the topographic shading delays the breakup, and other studies have shown that decreasing the surface heating rate in a valley can also delay the breakup (Bader and McKee 1985; Anquetin et al. 1998; Rendón et al. 2014). However, although the S–N valley is relatively colder as a consequence of more pronounced topographic shading, the breakup time does not exhibit a noticeable difference between both valleys. An explanation for this will be given in section 4.

Figure 5 shows the time–height evolution of θ in both valleys. For both valleys, this figure confirms that the

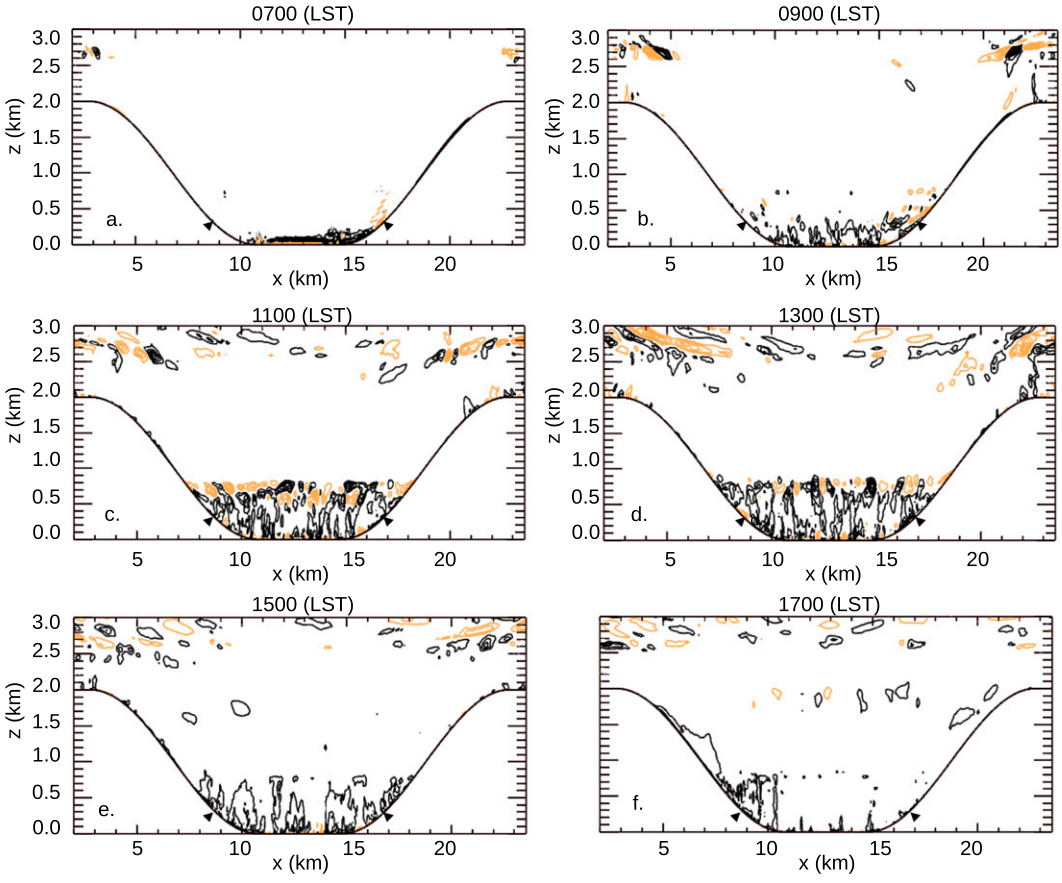

FIG. 2. Consecutive differences between the longitudinal mean fields of the cross-valley (θ) potential temperature in the S–N and E–W valleys: (top left) 0700 to (bottom right) 1700 LST. Isolines are shown every 0.04 K; negative and positive contours are black and orange, respectively. The black triangles in the outline of the orography mark the edges of the urban area.

breakup is mainly caused by the rise of the bottom of the inversion layer, and shows three main differences in the θ profiles between the center and the sidewalls. First, the heating rate is faster over the sidewalls than over the center owing to the upward movement of warm air along the slopes, both below and above the inversion layer (Fig. 8). Note, for instance, that below the inversion layer $296 < \theta < 297$ K at 1200 LST in the center, whereas $297 < \theta < 298$ K over the sidewalls. At the same time, above the inversion $298 < \theta < 299$ K while $\theta > 299$ K over the sidewalls. The upper part of the sidewalls reach $\theta = 299$ K before 0800 LST, while in most parts of the center profile this potential temperature is reached around 1600 LST. Second, the bottom of the inversion layer rises faster over the sidewalls than in the center, which is also owing to the upslope flow. For instance, at 1000 LST the height of the inversion layer bottom is ~0.60 km over the sidewalls, while in the center it is ~0.45 km. Third, the top of the inversion layer moves upward over the sidewalls but not in the center. For instance, from 1000 to 1200 LST, the height of the inversion top varies from ~0.80 to ~0.90 km over the sidewalls, while it remains approximately constant in the center. The ascent of the top of the inversion over the slopes is caused by the upslope flows and the ascending motions both below and above the edges of the inversion layer, while the constancy of the inversion-top height in the center is related to relatively weak vertical motions occurring above the inversion layer (Fig. 8).

Figures 3 and 5 also show the development of a shallow superadiabatic layer near the ground over the sidewalls of both valleys. Note, for instance, that at 1200 LST, there is a thin layer around $z = 0.3$ km where θ decreases with height, that is, a superadiabatic layer. This layer develops at 0900 LST and afterward near the rural–urban fringe, possibly as a result of the progressive heating of the surface and the sudden change in sensible heat flux on the sidewalls at the edges of the urban area. The appearance of such superadiabatic layer might be associated with the development of upslope winds that

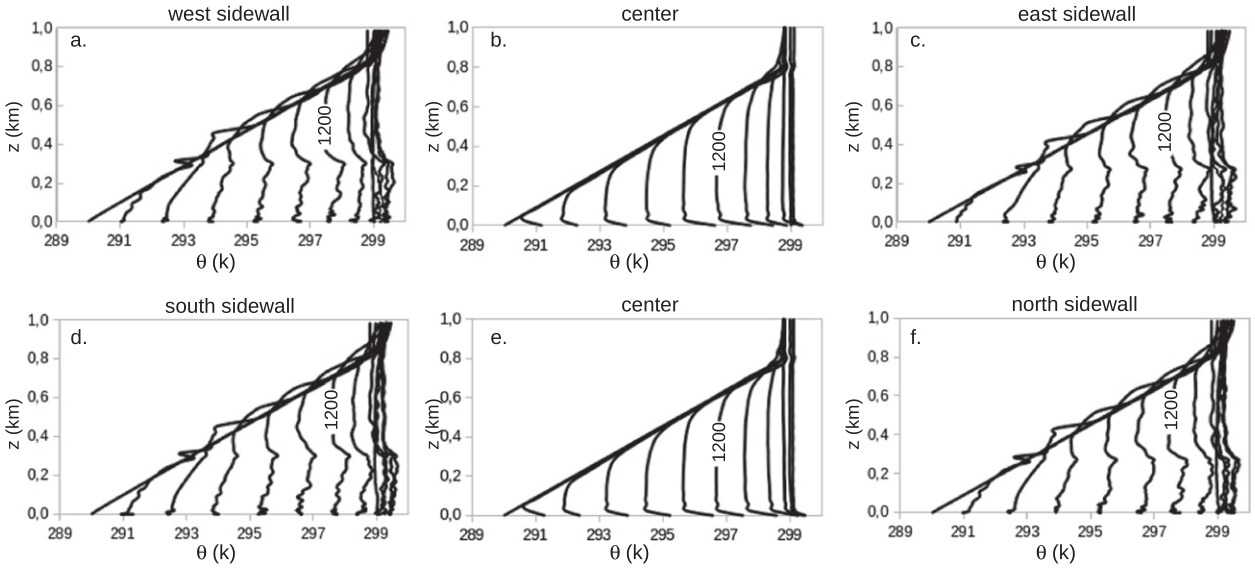

FIG. 3. Vertical θ profiles taken every hour from 0600 to 1800 LST in the (a)–(c) S–N and (d)–(f) E–W valleys, at (left) the left sidewall, (center) the midvalley, and (right) the right sidewall. Profiles in the sidewalls are taken along the slope (i.e., they are pseudovertical). In all panels, profiles evolve in time from the initial inversion profile to the left to the final well-mixed condition to the right.

remove air from the base of the inversion, as hypothesized by Whiteman and McKee (1977). Interestingly, in our results, the appearance of this superadiabatic layer coincides with the development of upslope winds (Fig. 8).

Figure 5 also shows an asymmetry in the time–height evolution of θ in the S–N valley. The upper part of the west sidewall is heated faster than the corresponding part of the east sidewall. Before 0700 LST, θ has exceeded 299 K in the west side while $\theta < 299$ K in most of the opposite east side. In contrast, the time–height evolution of θ in the E–W valley is substantially symmetric.

The differences in the time–height evolution of θ between both valleys are shown in Fig. 6. These differences are more pronounced along the sidewalls than in the center, and there are marked differences between the conditions below and above the inversion. The CBL (below the inversion) is generally colder in the S–N valley, although the differences exhibit random variations between positive and negative values owing to the turbulence within this layer. Above the inversion, the θ profiles evolve similarly in the center of both valleys but differently along the sidewalls. In contrast to the E–W valley, the upper part of the left sidewall of the S–N valley is more heated during the morning (orange contours in Fig. 6a) and less heated during the afternoon (black contours in Fig. 6a), whereas the right sidewall of the S–N valley is less heated during the morning (black contours in Fig. 6c) and similarly heated during the afternoon.

The location of the more marked differences between the θ fields of both valleys (Fig. 6) coincides with the space–time location of the greater differences in the surface heating (Fig. 1). However, during the afternoon, the increased heating of the upper part of the right sidewall of the S–N valley (Fig. 1) results in relatively smaller differences between θ in both valleys (note the small differences in the upper-right side of Fig. 6c). This suggests that the differences caused by the topographic effects on the heating of the right sidewall during the afternoon are reduced because at that time the cross-valley wind system has been well developed and it enhances the transport of heat throughout the valley. In contrast, during the early morning the cross-valley wind system is much less developed and, therefore, the differences between both valleys in the atmosphere heating are less dissipated by the mixing owing to the wind circulation.

Figure 7 shows the differences between the θ profiles over the center and over the sidewalls for each valley. Interestingly, the mean differences are on the same order of magnitude as the bias (~0.4 K) found by Whiteman et al. (2004) when comparing vertical soundings (in the center) and sidewall air temperature measurements (along the sidewalls, that is, pseudovertical profiles) in a small Alpine basin under stable nighttime conditions with low background winds. Furthermore, the smaller mean differences are below the top of the inversion ($z \sim$ 0.8 km), that is, within the stable layer. Whiteman et al. (2004) suggest that under high-static-stability conditions the pseudovertical profiles along the sidewalls can be good proxies for free air temperature soundings over the basin center. Our results lend support to this idea because

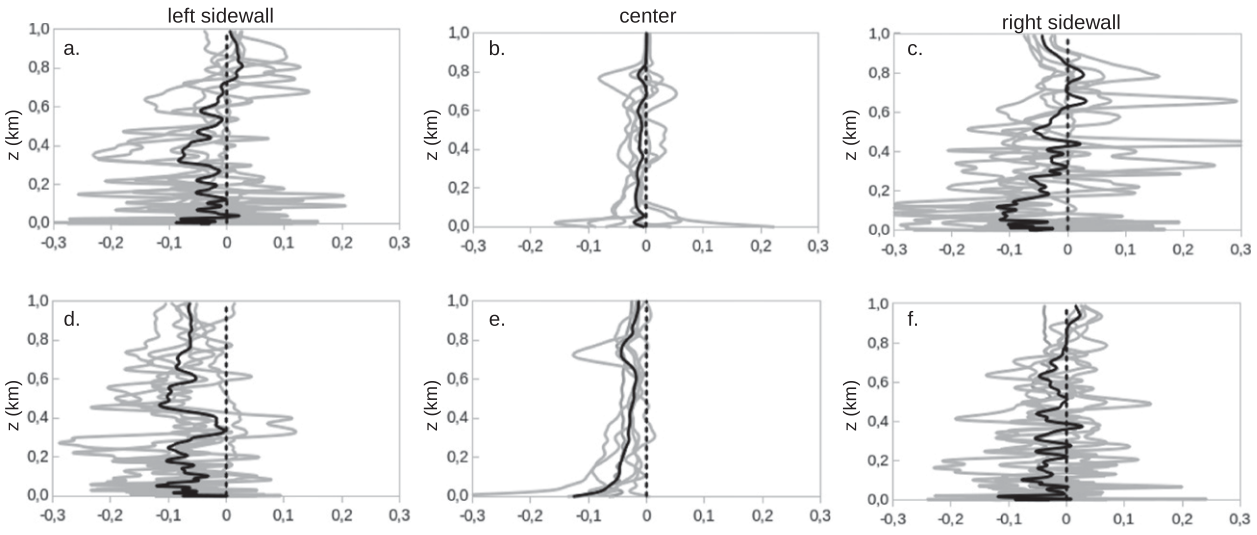

FIG. 4. Consecutive differences between the θ profiles in the S–N and E–W valleys (a)–(c) during the morning (from 0600 to 1200 LST) and (d)–(f) during the afternoon (from 1200 to 1800 LST). Differences are shown for the profiles in the center of the valley as well as in the left (west–south) and right (east–north) sidewalls. Each panel shows the hourly differences (gray lines) and the 6-h time average (black line). The dashed line indicates the zero difference value.

they show a similar correspondence between the center and sidewall profiles, despite our simulations having less stable conditions during the daytime.

b. Cross-valley wind system and thermal turbulence

The mean wind and resolved TKE fields in the cross section of both valleys, as well as the differences between them, are depicted every 3 h in Fig. 8 (vertical wind component w), Fig. 9 (horizontal wind component u), and Fig. 10 (resolved TKE). The mean circulation of both valleys is characterized by the development of (i) a CBL above the valley floor, (ii) slope winds, (iii) thermal plumes detaching from the mountaintops, (iv) a convergence zone toward the center of the valley in the upper atmosphere (~500 m above the mountaintops), and (v) circulations above and below the inversion layer.

In both valleys, the flow field over the valley floor is characterized by the presence of updrafts and downdrafts associated with thermal turbulence, whereas over the slopes it is characterized by the development of slope flows (Figs. 8 and 9). Figure 10 confirms that the production of thermal turbulence is more efficient over the valley floor, over the urban area, and over the mountaintops, which agrees with previous studies (e.g., Serafin and Zardi 2010a) and the understanding that urban areas, relative to their surrounding rural areas, are characterized by greatly enhanced production of thermal turbulence as a result of the increase in the surface heating and changes in stability accompanying the UHI (Oke 1995; Baklanov 2002). This production of thermal turbulence leads to the development of a CBL above the urban area located on the valley floor and over the lower part of the sidewalls, and thermal plumes detaching from the crests. The turbulent flow within the CBL exhibits a structure of convective circulations composed of updrafts (thermals) and downdrafts (Fig. 8), which is the expected structure that arises when turbulence generated by buoyancy due to upward heat flux from the surface dominates relative to turbulence generated by mean shear (Schmidt and Schumann 1989). The development of the CBL over the valley floor is weak during the early morning because of the low heating of the surface but becomes substantial afterward, which in turn greatly reduces the inversion layer from its bottom.

The flow in the thermal plumes is dominated by ascending motions (Fig. 8). These thermals are more intense during the early morning than they are during the late afternoon because of the dynamics of the slope winds. Upslope winds prevail during most of the daytime, which is the expected condition in mountain valleys (Whiteman 2000, p. 187), but in both valleys downslope winds develop in the late afternoon (1700 LST; Figs. 9p,q). This latter finding is in agreement with previous results that a UHI in a valley floor can induce downslope winds (Rendón et al. 2014; Savijärvi and Liya 2001). The mechanism that causes the downslope flows in both valleys during the late afternoon may be explained as follows. In the late afternoon the flow within the CBL developed over the valley floor is dominated by ascending motions (Figs. 8p,q), which is

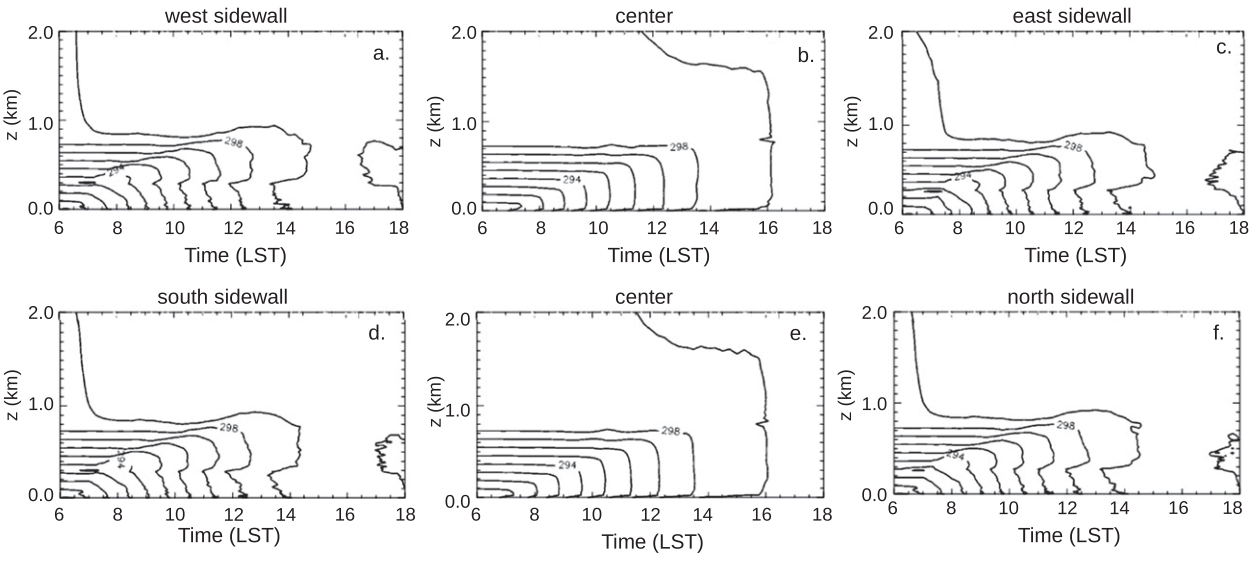

FIG. 5. Time–height variation of the θ profiles in the (a)–(c) S–N and (d)–(f) E–W valleys, at (left) the left sidewall, (center) the midvalley, and (right) the right sidewall. Isolines are shown every 1 K.

a consequence of the UHI in the core of the valley that creates thermal updrafts and, therefore, induces air convergence toward the valley center (Figs. 9p,q). In turn, this horizontal convergence is compensated by the downslope winds. This is also associated with the thermal differences inducing pressure gradients between the UHI in the valley floor and the predominantly rural valley sidewalls. This mechanism might be enhanced (the downslope winds may be stronger) if an inversion is present because it would restrict the ascending motions and, therefore, would induce a circulation below the inversion layer (see Fig. 3k of Rendón et al. 2014).

The restriction of the vertical motions caused by the inversion leads to a decoupling between the circulation below and above the inversion layer in both valleys. This decoupling effect owing to an inversion layer has been observed in several studies (Kalthoff et al. 1998; Argentini et al. 1999; Zhong et al. 2004; Li et al. 2009; Rendón et al. 2014), including a decoupling of the slope flows between the upper and lower parts of the slopes (Papadopoulos and Helmis 1999). As previously described, the flow field below the inversion layer is characterized by the growth of a CBL over the valley floor and by the slope winds. Above the inversion, the ascending motions in the thermal plumes are linked to a convergence zone aloft [~(500–1000) m] above the mountaintops; Fig. 9). Neglecting any net mass flux across the boundaries of the domain, as it is prescribed in the model experiment, mass continuity implies that these ascending motions and the associated horizontal convergence must be compensated by descending motions elsewhere. An expected flow pattern according to the BTI patterns proposed by Whiteman (1982) and Whiteman and McKee (1982) involves subsidence from above the inversion layer over the valley center. Our results show some subsidence in the valley center (Figs. 8j,k) but also over the sidewalls (Figs. 8d,e,g,h) and some ascending motions over the inversion layer (Figs. 8g,h). These ascending motions are associated with the circulation over the inversion that is shown in Figs. 9g,h. In both valleys, the subsidence from above the inversion layer does not play a significant role in the BTI, which is consistent with the profiles shown in Fig. 3 where the top of the inversion does not substantially descend.

Some of the turbulence produced within the thermal plumes is advected toward the center by the mean wind, thus leading to the formation of an elevated turbulent layer (Fig. 10), which is a process that has been noted and discussed in previous studies (Reuten et al. 2007; Serafin and Zardi 2010b,a). Figure 10 also confirms that the flow field within the inversion layer is characterized by weak turbulence associated with high stability.

Despite the common features described before, the turbulence and wind fields of the two valleys are different in several aspects. The differences between the vertical wind and turbulence fields of both valleys (Figs. 8c,f,i,l,o,r) are concentrated in the regions where the vertical motions are more intense and the production of thermal turbulence is more efficient, that is, within the CBL that develops over the valley floor and the thermal plumes that develop over the mountaintops. The differences vary randomly between positive and negative values, which is consistent with the turbulent nature of the flow in such regions, and are greater

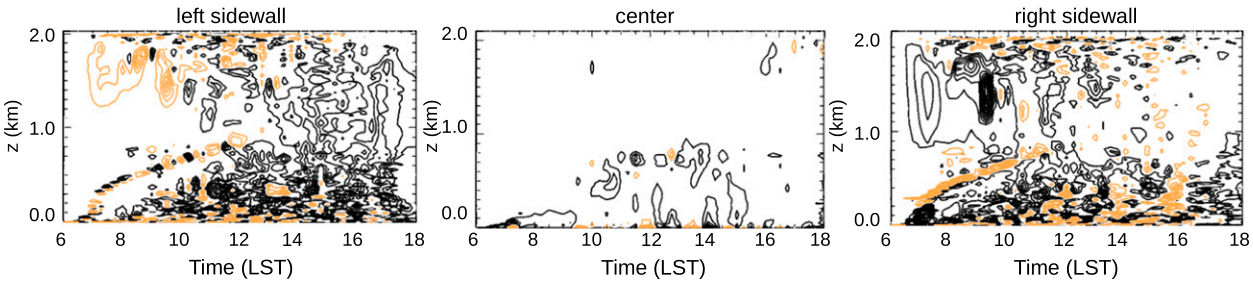

FIG. 6. Time variation of the differences between the θ profiles in the S–N and E–W valleys, at (left) the left sidewall, (center) the midvalley, and (right) the right sidewall. Isolines are shown every 0.04 K; negative and positive contours are black and orange, respectively.

(lesser) in the thermal plumes during the morning (afternoon) and in the CBL during the afternoon (morning), which coincides with the more intense development of the corresponding turbulent flows. The thermal plumes are more intense during the late morning (Figs. 8d,e,g,h and 10d,e,g,h) and have almost disappeared by the late afternoon (Figs. 8p,q and 10p,q), whereas the CBL is very shallow during the early morning (Figs. 8a,b,d,e and 10a,b,d,e) but has developed up to a height about coincident with the mountaintops by the late afternoon (Figs. 8p,q and 10p,q).

The symmetry of the flow field in the E–W valley is substantially maintained throughout the daytime owing to its symmetric topography and thermal forcing. In contrast, the asymmetric heating of the surface in the S–N valley leads to asymmetries, especially in the slope flows and the circulation above the inversion layer. During the early morning the region of ascending motions is larger over the east-facing slope (Fig. 8d), while in the late afternoon the upslope winds are more intense over the west-facing slope (Fig. 8p). The initial symmetry of the flow field in the S–N valley is also disrupted by the development of cross-valley flows over the inversion layer. There is an easterly flow at 1100 LST (Fig. 9g) and a westerly flow at 1300 LST (Fig. 9j). These flows are directed toward the sunlit-warmer sidewall, which agrees with the expected results of the conceptual experiment proposed by Lehner et al. (2011; recall their Fig. 1), and also with their observation that in Arizona's Meteor Crater the horizontal temperature and pressure gradients and wind directions change as the sun moves across the sky, with easterly and westerly winds before and after noon, respectively. However, there are some differences in our results with respect to that study that will be discussed in section 4. The circulation above the inversion in the S–N valley becomes more symmetric in the late afternoon than it was earlier, so the cross-valley flow disappears. This suggests a small asymmetry in the wind system during the afternoon, which we attribute to effects that will be discussed in section 4.

Another difference between both valleys is that, below the top of the inversion, the convergence of air toward the center of the city that occurs at the late afternoon is more intense in the S–N valley (Figs. 9p–r). Note that this is indicated by positive (negative) differences in the left (right) sidewall (Fig. 9r). We attribute this to a more intense UHI-induced circulation that occurs at the late afternoon in the core of the S–N valley, as compared with the E–W valley. This will be discussed in section 4.

c. *Transport of air pollutants*

The transport of a passive tracer continuously emitted from the urban area is depicted in Fig. 11. This figure shows the mixing ratio of the tracer (milligram of tracer per kilogram of dry air) for both valleys. The tracer is emitted only from the urban area, and in these areas the surface flux is given by $17\,\mathrm{kg\,h^{-1}\,km^{-2}}$. At each time step, a corresponding amount of tracer is added to the lowest grid box. The resulting mixing ratio χ is then advected by the flow according to $D\chi/Dt = 0$, where D/Dt denotes the material derivative. The chosen surface flux is based on measurements of annual carbon emissions from an urban area of about $360\,\mathrm{km^2}$ in the Aburrá river valley in Colombia (Toro et al. 2001). Note that the amount of pollutant released to the atmosphere grows linearly both with time and with the size of the urban area.

In both valleys, the capping effect of the inversion layer is confirmed by Fig. 11, where the pollutant emitted from the urban area remains substantially trapped below the inversion. This agrees well with a number of experimental and modeling studies (e.g., Anquetin et al. 1999; Savijärvi and Liya 2001; Sokhi et al. 2002; Berge et al. 2002; Reuten et al. 2005; Steyn et al. 2013). In particular, there is an accumulation of pollutants over the lower part of the sidewalls, which is a situation that can be described as a "smog trap" and is likely to occur in an urban valley as a result of the interplay between the slope flow, a temperature inversion, and a UHI (Savijärvi and Liya 2001). This smog trap is similar to that found for a less deep

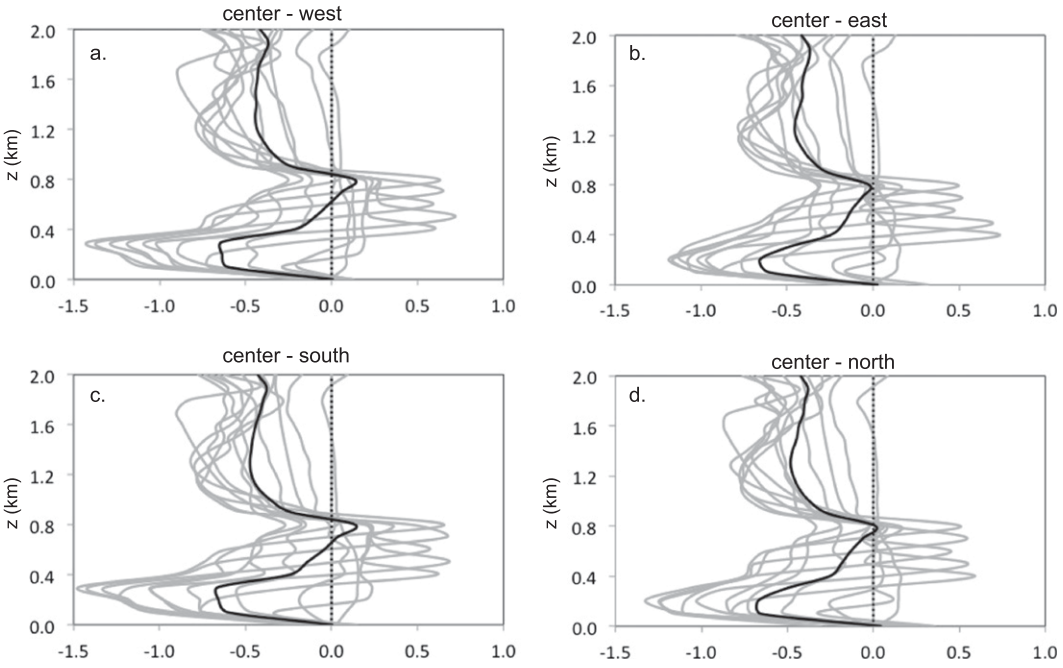

FIG. 7. Consecutive differences between the θ profiles in the center and along the sidewalls of the (a),(b) S–N and (c),(d) E–W valleys. Each panel shows the hourly differences (gray lines) and the 12-h time average (black line). The dotted line indicates the zero difference value.

urban valley (Rendón et al. 2014), but the mechanism causing the present smog trap is different. In that previous study the smog trap found over the slopes was associated with a circulation below the inversion layer that consists of downslope winds and their partial recirculation toward the slopes owing to the restriction of vertical motions caused by the inversion layer. The smog trap shown in Fig. 11 is also caused by a circulation below the inversion layer but in the opposite direction (Figs. 8 and 9). While the inversion persists, the upslope winds from the valley floor are deviated toward the center of the valley because of the inversion layer (see, e.g., Lehner and Gohm 2010). Some descending winds below the inversion close a circulation, which explains why a substantial amount of pollutants may remain trapped over the slopes before the BTI. The mixing ratio of air pollutants over the slopes and below the inversion is also increased because such pollutants are diluted in a smaller volume than the corresponding volume below the inversion in the center of the valley.

After the BTI, the pollutants are gradually vented out of the valley by the slope winds and the turbulent flow within the growing CBL. Nevertheless, a substantial amount of pollutants remains over the city during the late afternoon. Figures 11m–o show that the air over the urban area is more polluted in the S–N valley (this is indicated by the positive differences in the valley floor in Fig. 11o), and that in the E–W valley more pollutants are transported up to 1000–1500 m above the valley floor (this is indicated by the negative differences in Fig. 11o). As a result, in the E–W valley, as compared to the S–N valley, there is an elevated polluted layer at 1500 LST resulting from the more efficient transport of pollutants by the upslope winds and convection near the slopes. Later, it turns out that the upper part of the left sidewall of the E–W valley is more polluted than the corresponding sidewall of the S–N valley (this is indicated by the negative differences in Fig. 11r), while the right sidewall is more polluted in the latter valley (this is indicated by the positive differences in Fig. 11r). This is because the mass flux in the upslope wind is larger above the right (left) sidewall of the S–N (E–W) valley in the late afternoon (Figs. 9p,q). However, the smog trap in the lower part of the left sidewall, over the urban area, remains more polluted in the S–N valley. We associate this with a stronger UHI-induced circulation in the S–N valley, which, in turn, is owing to the shading.

Together the previous results indicate that the pollutants are more efficiently vented out of the urban area in the E–W valley, that is, that the topographic effects on reducing the surface heating of the S–N valley, as compared with the E–W valley, tend to restrict more the ventilation of the former. This generally agrees with previous results that the reduction of the absorbed solar radiation at the surface causes

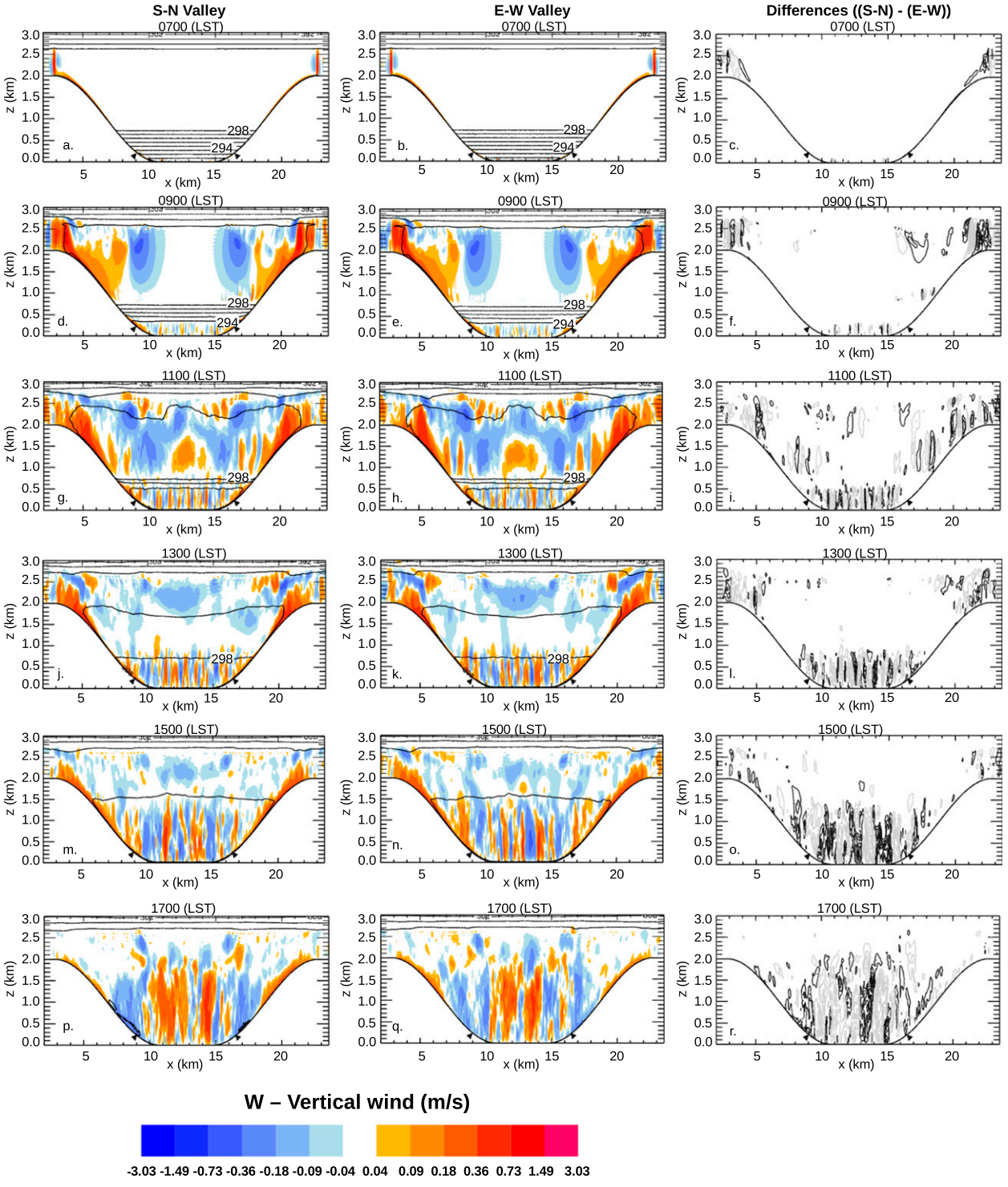

FIG. 8. Consecutive longitudinal mean fields of the cross-valley w in the (left) S–N and (center) E–W valleys, and (right) differences between both valleys: from 0700 to 1700 LST. Isentropes are shown every 1 K. Contours for differences are every 0.1 m s^{-1}. The black triangles in the outline of the orography mark the edges of the urban area.

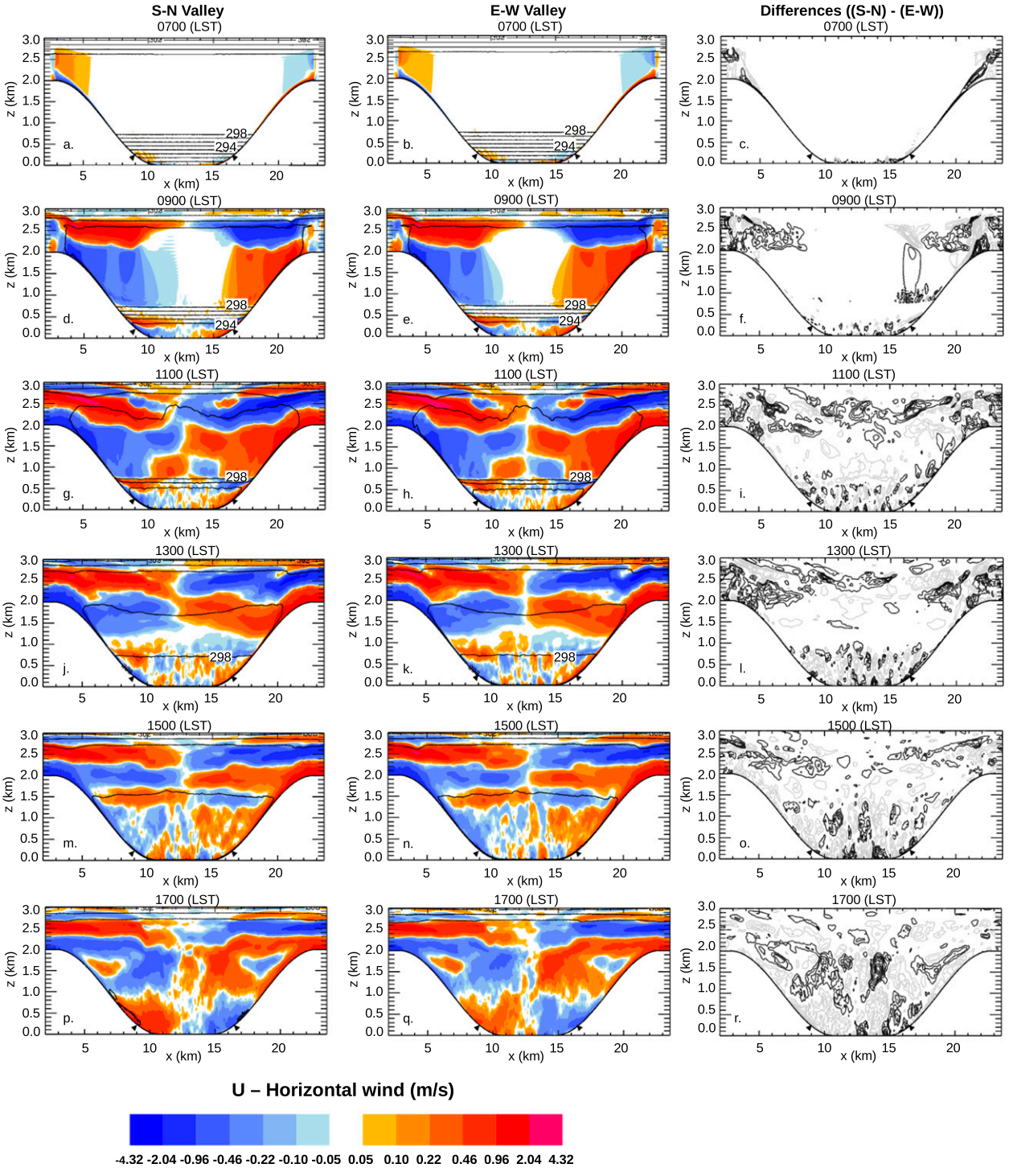

FIG. 9. As in Fig. 8, but for u.

a reduction of the mass flux in the slope-wind layer, thereby restricting the valley ventilation (Lehner and Gohm 2010). The mechanisms of air pollution transport in the valleys will be further discussed in the following section.

4. Discussion

In this section we discuss (i) the processes driving the BTI, (ii) the implications of the topographic effects on the surface heating depending on the orientation of

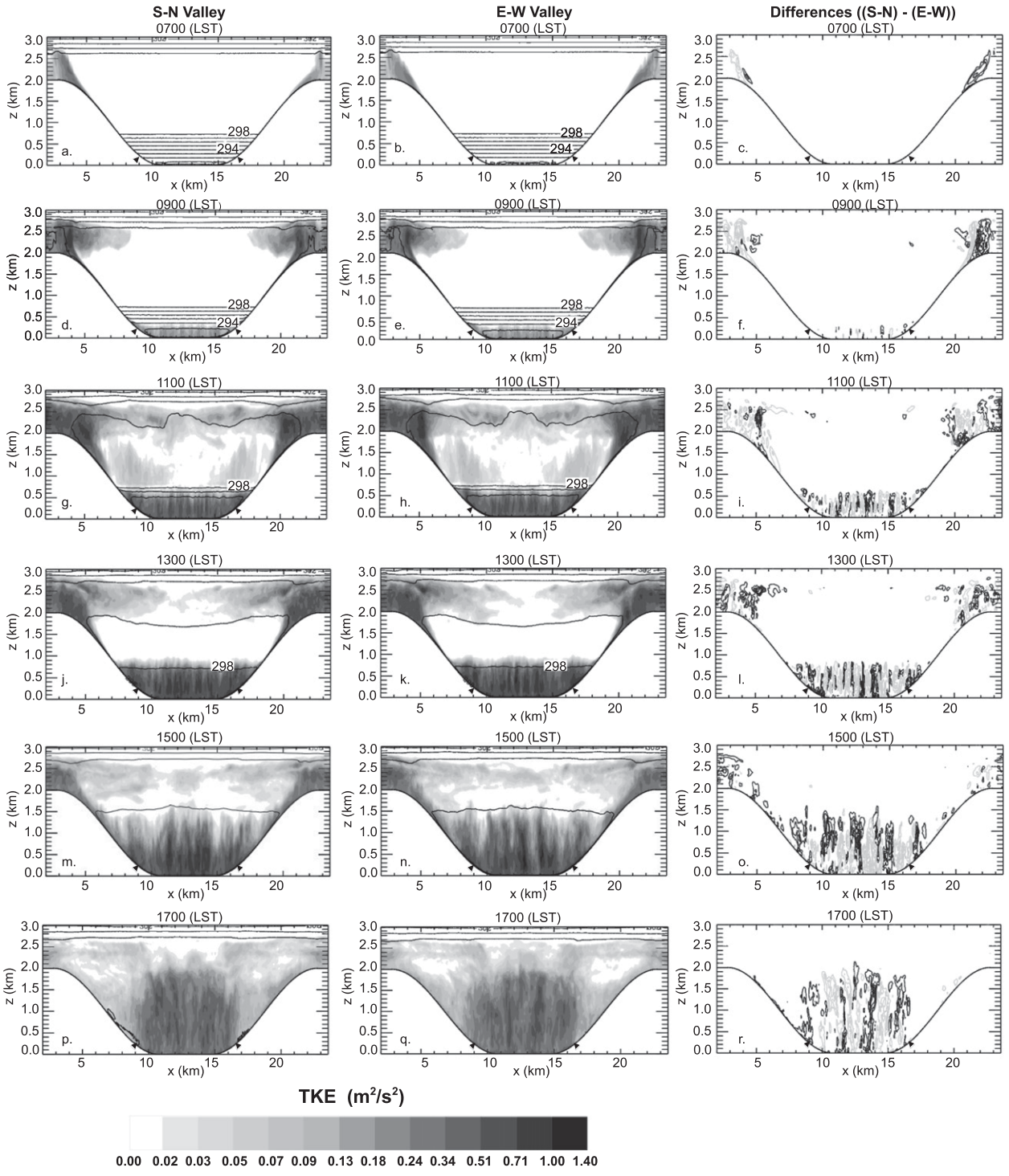

FIG. 10. As in Fig. 8, but for resolved TKE. Contours for differences are every 0.08 $m^2 s^{-2}$.

the valley, and (iii) the mechanisms of air pollution transport. Figure 12 summarizes the evolution in time of the flow field, the inversion layer, and the tracer distribution observed in this study.

The process that dominates the BTI is the production of thermal turbulence at the valley floor, which leads to the development of a CBL, in turn causing the rise of the bottom of the inversion layer. The height of the inversion

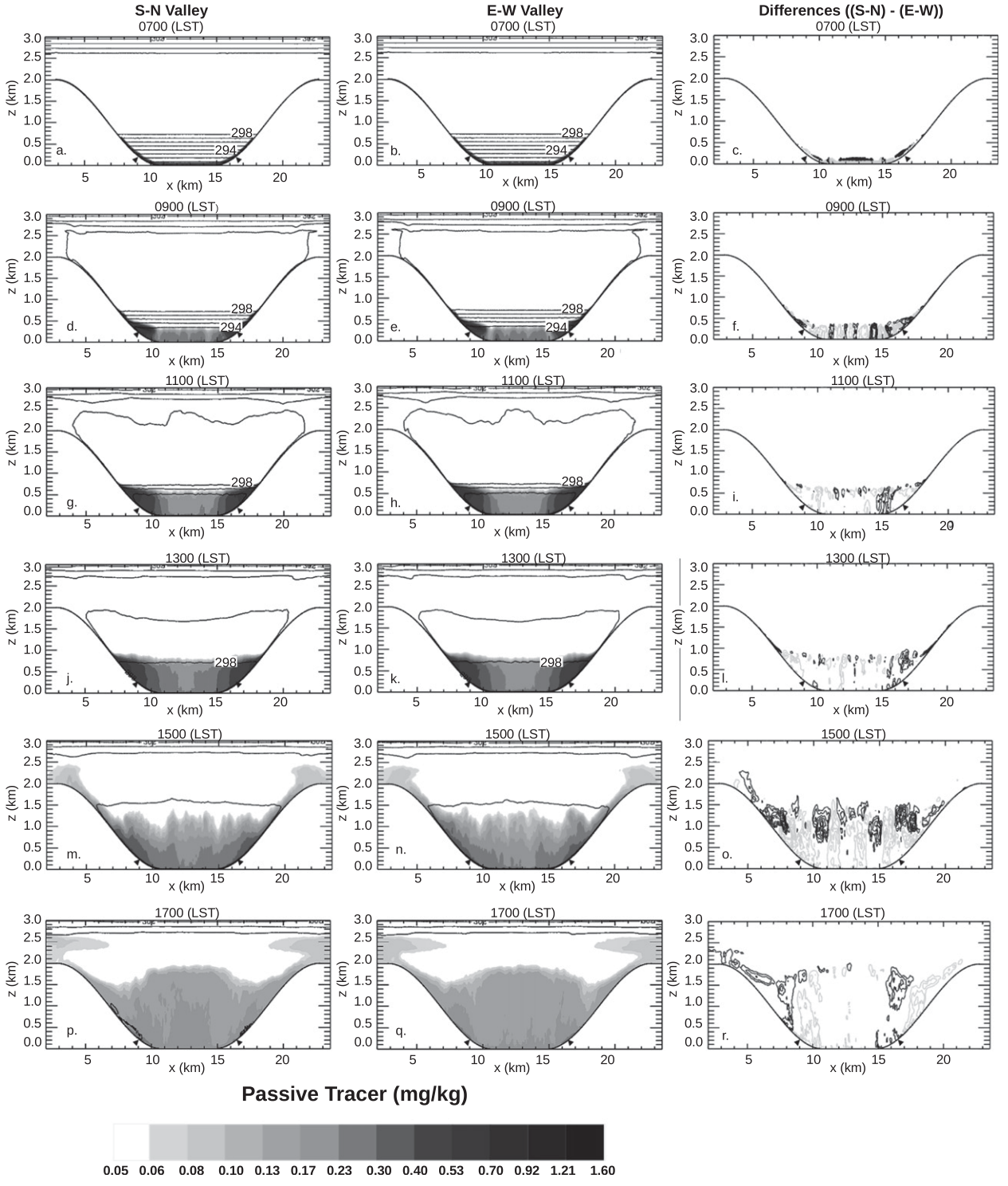

FIG. 11. Passive tracer mixing ratio (mg kg^{-1}) in the (left) S–N and (center) E–W valleys (see text for details), and (right) differences between both valleys: from 0700 to 1700 LST. Isentropes are shown every 1 K. Contours for differences are every 0.02 mg kg^{-1}. The black triangles in the outline of the orography mark the edges of the urban area.

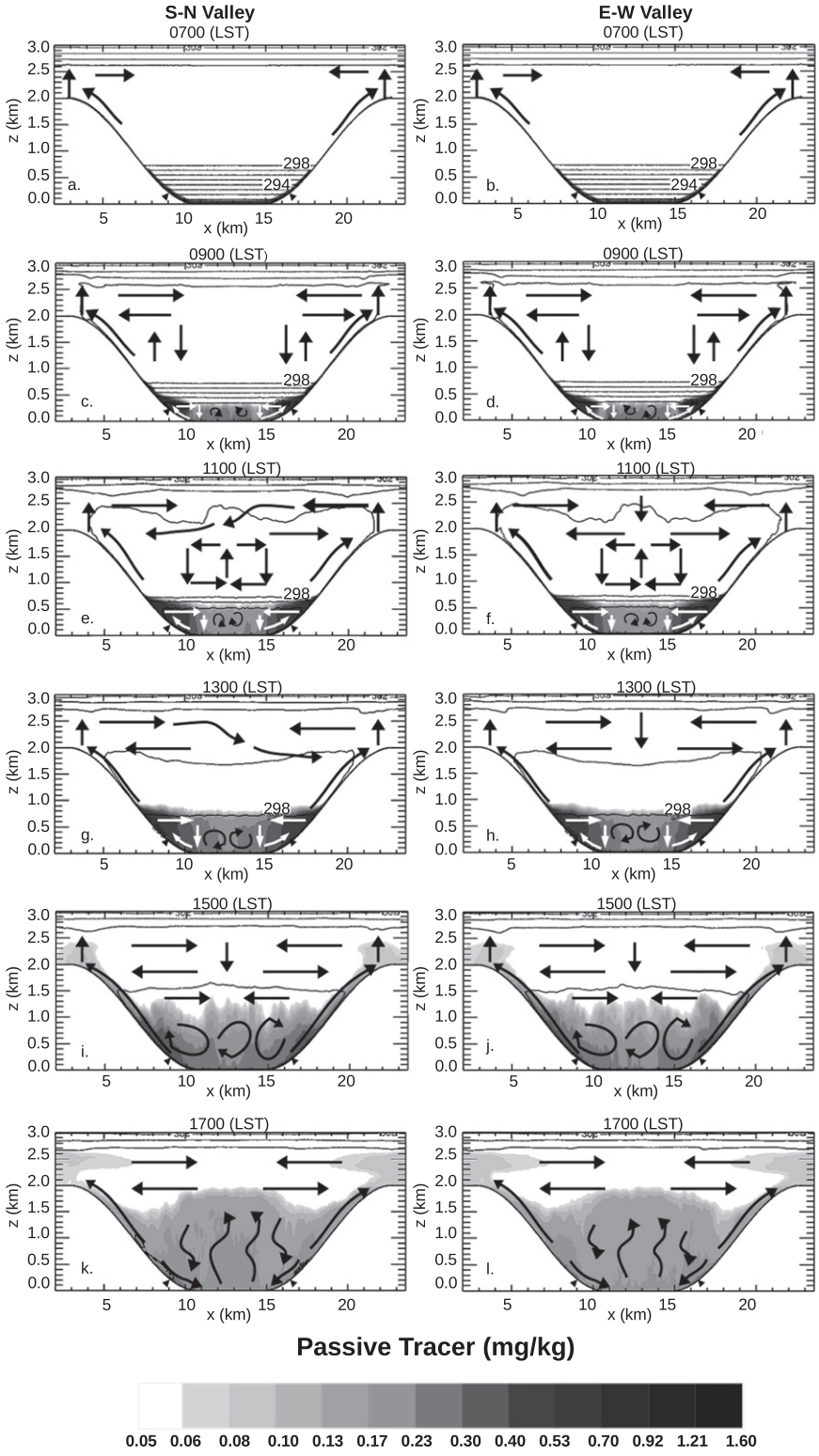

FIG. 12. Schematic of the evolution in time of the flow field associated with the tracer distribution for (left) S–N and (right) E–W valleys: from 0700 to 1700 LST. Arrows indicate mean flow and turbulent eddies. The shading indicates the tracer mixing ratio as in Fig. 11. Isentropes are shown every 1 K.

top does not change very much during the BTI. This is characteristic of the BTI pattern 1 according to Whiteman (1982) and Whiteman and McKee (1982), and agrees with the BTI pattern found for a less steep similarly urbanized valley in Rendón et al. (2014) (see Fig. 6c of this study). Other possible BTI patterns would be patterns 2 and 3. In pattern 2 the BTI is dominated by the descent of the top of the inversion layer caused by the removal of air from the bottom of the valley by the upslope winds, and the air subsidence from the upper atmosphere; while in pattern 3 the BTI is caused by the combined effect of both processes, the ascent of the bottom of the inversion layer associated with the CBL and the descent of its top linked to the upslope winds and the air subsidence above the inversion layer. The absence of patterns 2 and 3 in our results may be explained by two factors. First, the UHI increases the heating of the valley floor, thus enhancing the growth of a CBL, which is a process that does not substantially occur in pattern 2. Second, both patterns 2 and 3 imply that the upslope winds are strong enough to substantially remove air from the base of the inversion and so to induce subsidence from above the inversion. In our simulations, the development of the CBL is not that weak owing to the presence of the UHI, and the upslope winds are not that strong because of the relatively low heating of the sidewalls and the capping effect of the inversion. Furthermore, the circulation above the inversion not only involves weak subsidence but also some ascending motions (Figs. 8g,h).

The orientation of a valley with respect to the sun may lead to asymmetric heating of the sidewalls and topographic shading, that is, topographic effects on surface heating. The main implications of these effects observed in previous studies are (i) a delay of the BTI as a consequence of the topographic shading (Colette et al. 2003); (ii) an asymmetric evolution of the slope flows; and (iii) the development of cross-valley winds either in the presence or absence of a temperature inversion, and both above and below an inversion layer. Furthermore, the asymmetries in the flow field lead to an asymmetric distribution of pollutants (Gohm et al. 2009; Lehner and Gohm 2010; Lehner et al. 2011). In contrast to these studies, our results show neither a delay in the BTI as a consequence of the topographic shading nor strong asymmetries in the flow field and tracer distribution. Although our results show some asymmetries, they are not so strong as to cause cross-valley flow below the inversion (see, e.g., Figs. 1 and 10 of Lehner et al. 2011) or a very pronounced asymmetric tracer distribution owing to a strong mass flux in the upslope wind of one but not both sidewalls [e.g., see Fig. 10c of Gohm et al. (2009) and Fig. 3 of Lehner and Gohm (2010)]. We attribute this to two factors. First, the valleys in our simulations are both located at the equator, so the topographic shading is generally less pronounced than it would be in higher latitudes, especially in winter. This means that the asymmetry between the surface heating of the east- and west-facing slopes in the S–N valley (Fig. 1) is less pronounced than that suggested, for instance, in Fig. 1 of Lehner et al. (2011). Second, the development of the cross-valley wind system, and particularly of the CBL over the UHI, favors the mixing of the atmosphere (this is what we have called a ''mixing effect''). The absence of cross-valley flow below the inversion despite the asymmetric heating of the sidewalls in the S–N valley can be explained by the effects of the UHI in producing thermal turbulence and the associated development of a CBL, thereby favoring the mixing below the inversion layer. Furthermore, there is a UHI-induced circulation whose interplay with the inversion layer causes closed circulations (smog traps) below the inversion, particularly over the lower parts of the sidewalls. The study of Lehner et al. (2011) does not consider a UHI on the valley floor.

Our results illustrate three types of interconnected mechanisms of air pollution transport. Type A describes the transport of pollutants by upslope winds. This mechanism is dominated by thermal forcing due to solar irradiation and has been found to be particularly important under weak synoptic and mesoscale pressure gradients (Gohm et al. 2009). Type B describes the transport caused by the UHI-induced circulation, characterized by the occurrence of downslope winds in the late afternoon. Type C describes the transport within a closed slope-flow circulation below the inversion layer, which results in what we have called a smog trap that occurs in the lower part of the sidewalls. Mechanisms comparable to types B and C have been found in previous studies (e.g., Savijärvi and Liya 2001; Reuten et al. 2005; Rendón et al. 2014).

The transport of pollutants by upslope winds (type A) is strongly restricted by the inversion layer, which causes a decoupling between the slope flows in the upper and lower parts of the sidewalls. Before the breakup (Figs. 12a–h), upslope flows develop in the upper parts of the sidewalls but they do not transport the pollutants that remain substantially trapped below the inversion. In this situation the inversion layer reduces the mass flux in the slope wind layer (Vergeiner and Dreiseitl 1987). After the breakup (Figs. 12i,j), upslope flows develop from the bottom to the top of the sidewalls, thus venting pollutants out of the valley floor to the mountaintops and beyond. In the late afternoon (Figs. 12k,l) the slope flow becomes decoupled again with upslope and downslope winds in the upper and lower parts of the sidewalls, respectively. This decoupling is not caused by the inversion

layer but rather by the influence of the UHI on the low-level circulation (type B).

A UHI-induced circulation (type B) dominates the flow field above the valley floor during the late afternoon (Figs. 12k,l). The UHI induces convergence (Figs. 9p,q) and rising motions (Figs. 8p,q) over the heat source, which in turn are compensated by downslope winds. This downslope flow occurs in the late afternoon because at that time the convergence induced by the UHI dominates over the effect of the sidewall heating in creating upslope winds. The heating of the lower part of the sidewalls in the late afternoon is reduced by the influence of topography. The downslope winds restrict the ventilation of the valley floor through the sidewalls, whereas the updrafts in the core of the valley transport pollutants from the valley floor upward. Under these conditions, the ventilation of the valley would be worse if the inversion layer were not broken and, therefore, a closed circulation could develop below the inversion layer (see Fig. 8 of Rendón et al. 2014).

The trapping of pollutants within a closed circulation, that is, a smog trap (type C), is shown in Figs. 12c–h. Smog traps occur below the inversion layer in the lower part of the sidewalls. The upslope flows that develop below the inversion are decoupled from those developed above the inversion and are deviated toward the center of the valley. In turn, the resulting horizontal flows below the inversion layer (Figs. 9d,e,g,h,j,k) are restricted by the CBL. Therefore, descending flows near the base of the sidewalls (Figs. 8d,e,g,h,j,k) close the circulation that causes the smog trap. The persistence of this smog trap depends on the presence of the inversion layer, so the smog trap is disrupted when the inversion layer is broken.

5. Conclusions

Idealized simulations were analyzed to elucidate the breakup of an inversion layer in urban valleys subject to a strong low-level temperature inversion and topographic effects on surface heating, as well as the associated air pollution transport mechanisms. The following conclusions are drawn from our results:

(i) In tropical urban valleys, the orientation of the valley with respect to the sun may lead to small asymmetries in the flow field and pollutant distributions, as compared to those reported in previous studies for valleys located in higher latitudes, particularly in winter. Depending on the orientation of the valley, the topographic shading varies and can be reduced as the valley approaches the equator. This is an effect of latitude additional to, for instance, the effect of the Coriolis force.

(ii) In urban valleys subject to low-level temperature inversions the growth of a CBL over a UHI is expected to be the dominant process in the BTI, owing to the efficient production of thermal turbulence over the highly heated urban area.

(iii) The presence and evolution in time of a low-level temperature inversion strongly influences the dispersion of pollutants in urban valleys. UHIs are likely to develop in those valleys. The interaction between an inversion layer and the UHI may result in different mechanisms of air pollution transport. Three mechanisms were identified based on the results of present study (section 4). These are transport by upslope winds (type A), transport by the UHI-induced circulation (type B), and transport within a closed slope-flow circulation below an inversion layer (type C).

(iv) Populated areas located near the base of the sidewalls of urban valleys may be affected by the trapping of pollutants within a closed slope-flow circulation below an inversion layer, that is, a smog trap, which is likely to occur in the lower part of the slopes.

Acknowledgments. We gratefully thank B. Brötz for his help with the EULAG model, R. Bellasio for his help with his algorithm, and C. D. Whiteman for his most valuable comments and suggestions. We also thank J. F. Mejía, J. E. Cañón, Editor Joseph Charney, and the anonymous reviewers for their constructive comments. The computations for this study were performed in the supercomputer Blizzard in the German Climate Computing Center (Deutsches Klimarechenzentrum). Author AMR gratefully thanks the German Academic Exchange Service, DAAD, for supporting her as a visiting doctoral student in Germany through the short-term scholarship code A/10/77699 and the Colombian Administrative Department of Science, Technology and Innovation, COLCIENCIAS, for funding her doctoral studies through the research project ''Caracterización de procesos físicos en la baja atmósfera del Valle de Aburrá'' (código: 1115-48925515, contrato: 458-09) and Grant ''Francisco José de Caldas.''

REFERENCES

Anquetin, S., C. Guilbaud, and J. Chollet, 1998: The formation and destruction of inversion layers within a deep valley. *J. Appl. Meteor.,* **37,** 1547–1560, doi:10.1175/1520-0450(1998)037<1547:TFADOI>2.0.CO;2.

——, ——, and ——, 1999: Thermal valley inversion impact on the dispersion of a passive pollutant in a complex mountainous area. *Atmos. Environ.,* **33,** 3953–3959, doi:10.1016/S1352-2310(99)00137-5.

Argentini, S., G. Mastrantonio, and F. Lena, 1999: Case studies of the wintertime convective boundary-layer structure in the urban area of Milan, Italy. *Bound.-Layer Meteor.,* **93,** 253–267, doi:10.1023/A:1002057414039.

Bader, D. C., and T. B. McKee, 1985: Effects of shear, stability and valley characteristics on the destruction of temperature inversions. *J. Climate Appl. Meteor.,* **24,** 822–832, doi:10.1175/1520-0450(1985)024<0822:EOSSAV>2.0.CO;2.

Baklanov, A., 2002: The mixing height in urban areas——A review. *Proc. Mixing Height and Inversions in Urban Areas, COST Action 715, EUR 20451,* Toulouse, France, European Commission, 9–28.

Bellasio, R., G. Maffeis, J. Scire, M. Longoni, R. Bianconi, and N. Quaranta, 2005: Algorithms to account for topographic shading effects and surface temperature dependence on terrain elevation in diagnostic meteorological models. *Bound.-Layer Meteor.,* **114,** 595–614, doi:10.1007/s10546-004-1670-6.

Berge, E., A. Karppinen, J. Kukkonen, M. Køltzow, and L. Slørdal, 2002: Simulations of wintertime inversions in northern European cities by use of NWP-models. *Proc. Mixing Height and Inversions in Urban Areas, COST Action 715, EUR 20451,* Toulouse, France, European Commission, 75–88.

Chu, P. C., Y. Chen, S. Lu, Z. Li, and Y. Lu, 2008: Particulate air pollution in Lanzhou China. *Environ. Int.,* **34,** 698–713, doi:10.1016/j.envint.2007.12.013.

Colette, A., F. Chow, and R. Street, 2003: A numerical study of inversion-layer breakup and the effects of topographic shading in idealized valleys. *J. Appl. Meteor.,* **42,** 1255–1272, doi:10.1175/1520-0450(2003)042<1255:ANSOIB>2.0.CO;2.

Colvile, R., E. Hutchinson, J. Mindell, and R. Warren, 2001: The transport sector as a source of air pollution. *Atmos. Environ.,* **35,** 1537–1565, doi:10.1016/S1352-2310(00)00551-3.

Deardorff, J. W., 1980: Stratocumulus-capped mixed layers derived from a three-dimensional model. *Bound.-Layer Meteor.,* **18,** 495–527, doi:10.1007/BF00119502.

Gohm, A., and Coauthors, 2009: Air pollution transport in an alpine valley: Results from airborne and ground-based observations. *Bound.-Layer Meteor.,* **131,** 441–463, doi:10.1007/s10546-009-9371-9.

Grimmond, S., and T. Oke, 2002: Turbulent heat fluxes in urban areas: Observations and a local-scale urban meteorological parameterization scheme (LUMPS). *J. Appl. Meteor.,* **41,** 792–810, doi:10.1175/1520-0450(2002)041<0792:THFIUA>2.0.CO;2.

Haeger-Eugensson, M., and B. Holmer, 1999: Advection caused by the urban heat island circulation as a regulating factor on the nocturnal urban heat island. *Int. J. Climatol.,* **19,** 975–988, doi:10.1002/(SICI)1097-0088(199907)19:9<975::AID-JOC399>3.0.CO;2-J.

Hay, J. E., and D. C. McKay, 1985: Estimating solar irradiance on inclined surfaces: A review and assessment of methodologies. *Int. J. Sol. Energy,* **3,** 203–240, doi:10.1080/01425918508914395.

Hoch, S. W., and C. Whiteman, 2010: Topographic effects on the surface radiation balance in and around Arizona's Meteor Crater. *J. Appl. Meteor. Climatol.,* **49,** 1114–1128, doi:10.1175/2010JAMC2353.1.

Janhall, S., K. Olofson, P. Andersson, J. Pettersson, and M. Hallquist, 2006: Evolution of the urban aerosol during winter temperature inversion episodes. *Atmos. Environ.,* **40,** 5355–5366, doi:10.1016/j.atmosenv.2006.04.051.

Jung, M., and Coauthors, 2011: Global patterns of land–atmosphere fluxes of carbon dioxide, latent heat, and sensible heat derived from eddy covariance, satellite, and meteorological observations. *J. Geophys. Res.,* **116,** G00J07, doi:10.1029/2010JG001566.

Kalthoff, N., H. Binder, M. Kossmann, R. Vögtlin, U. Corsmeier, F. Fiedler, and H. Schlager, 1998: Temporal evolution and spatial variation of the boundary layer over complex terrain. *Atmos. Environ.,* **32,** 1179–1194, doi:10.1016/S1352-2310(97)00193-3.

Lehner, M., and A. Gohm, 2010: Idealised simulations of daytime pollution transport in a steep valley and its sensitivity to thermal stratification and surface albedo. *Bound.-Layer Meteor.,* **134,** 327–351, doi:10.1007/s10546-009-9442-y.

——, C. Whiteman, and S. W. Hoch, 2011: Diurnal cycle of thermally driven cross-basin winds in Arizona's Meteor Crater. *J. Appl. Meteor. Climatol.,* **50,** 729–744, doi:10.1175/2010JAMC2520.1.

Li, Y., R. Smith, and V. Grubišic, 2009: Using surface pressure variations to categorize diurnal valley circulations: Experiments in Owens Valley. *Mon. Wea. Rev.,* **137,** 1753–1769, doi:10.1175/2008MWR2495.1.

Malek, E., T. Davis, R. S. Martin, and P. J. Silva, 2006: Meteorological and environmental aspects of one of the worst national air pollution episodes (January, 2004) in Logan, Cache Valley, Utah, USA. *Atmos. Res.,* **79,** 108–122, doi:10.1016/j.atmosres.2005.05.003.

Matzinger, N., M. Andretta, E. Gorsel, R. Vogt, A. Ohmura, and M. Rotach, 2003: Surface radiation budget in an Alpine valley. *Quart. J. Roy. Meteor. Soc.,* **129,** 877–895, doi:10.1256/qj.02.44.

Nadeau, D. F., and Coauthors, 2009: Estimation of urban sensible heat flux using a dense wireless network of observations. *Environ. Fluid Mech.,* **9,** 635–653, doi:10.1007/s10652-009-9150-7.

Offerle, B., S. Grimmond, K. Fortuniak, and W. Pawlak, 2006: Intraurban differences of surface energy fluxes in a central European city. *J. Appl. Meteor. Climatol.,* **45,** 125–136, doi:10.1175/JAM2319.1.

Ogura, Y., and N. Phillips, 1962: Scale analysis of deep and shallow convection in the atmosphere. *J. Atmos. Sci.,* **19,** 173–179, doi:10.1175/1520-0469(1962)019<0173:SAODAS>2.0.CO;2.

Oke, T., 1995: The heat island of the urban boundary layer: Characteristics, causes and effects. *Wind Climate in Cities,* J. E. Cernak et al., Eds., Kluwer Academic, 81–107.

Oliphant, A., R. SpronkeN–Smith, A. Sturman, and I. Owens, 2003: Spatial variability of surface radiation fluxes in mountainous terrain. *J. Appl. Meteor.,* **42,** 113–128, doi:10.1175/1520-0450(2003)042<0113:SVOSRF>2.0.CO;2.

Papadopoulos, K., and C. Helmis, 1999: Evening and morning transition of katabatic flows. *Bound.-Layer Meteor.,* **92,** 195–227, doi:10.1023/A:1002070526425.

Prusa, J., P. Smolarkiewicz, and A. Wyszogrodzki, 2008: EULAG, a computational model for multiscale flows. *Comput. Fluids,* **37,** 1193–1207, doi:10.1016/j.compfluid.2007.12.001.

Rampanelli, G., D. Zardi, and R. Rotunno, 2004: Mechanisms of up-valley winds. *J. Atmos. Sci.,* **61,** 3097–3111, doi:10.1175/JAS-3354.1.

Rendón, A. M., J. F. Salazar, C. A. Palacio, V. Wirth, and B. Brötz, 2014: Effects of urbanization on the temperature inversion breakup in a mountain valley with implications on air quality. *J. Appl. Meteor. Climatol.,* **53,** 840–858, doi:10.1175/JAMC-D-13-0165.1.

Reuten, C., D. Steyn, K. Strawbridge, and P. Bovis, 2005: Observations of the relation between upslope flows and the convective boundary layer in steep terrain. *Bound.-Layer Meteor.,* **116,** 37–61, doi:10.1007/s10546-004-7299-7.

——, ——, and S. Allen, 2007: Water tank studies of atmospheric boundary layer structure and air pollution transport in upslope flow systems. *J. Geophys. Res.,* **112,** D11114, doi:10.1029/2006JD008045.

Rosenzweig, C., W. Solecki, S. Hammer, and S. Mehrotra, 2010: Cities lead the way in climate-change action. *Nature,* **467,** 909–911, doi:10.1038/467909a.

Rutllant, J., and R. Garreaud, 1995: Meteorological air pollution potential for Santiago, Chile: Towards an objective episode forecasting. *Environ. Monit. Assess.,* **34,** 223–244, doi:10.1007/BF00554796.

Savijärvi, H., and J. Liya, 2001: Local winds in a valley city. *Bound.-Layer Meteor.,* **100,** 301–319, doi:10.1023/A:1019215031007.

Schmidli, J., and Coauthors, 2011: Intercomparison of mesoscale model simulations of the daytime valley wind system. *Mon. Wea. Rev.,* **139,** 1389–1409, doi:10.1175/2010MWR3523.1.

Schmidt, H., and U. Schumann, 1989: Coherent structure of the convective boundary layer derived from large-eddy simulations. *J. Fluid Mech.,* **200,** 511–562, doi:10.1017/S0022112089000753.

Serafin, S., and D. Zardi, 2010a: Daytime heat transfer processes related to slope flows and turbulent convection in an idealized mountain valley. *J. Atmos. Sci.,* **67,** 3739–3756, doi:10.1175/2010JAS3428.1.

——, and ——, 2010b: Structure of the atmospheric boundary layer in the vicinity of a developing upslope flow system: A numerical model study. *J. Atmos. Sci.,* **67,** 1171–1185, doi:10.1175/2009JAS3231.1.

Sokhi, R., L. Luhana, J. Kukkonen, E. Berge, L. Slördal, and S. Finardi, 2002: Analysis of air pollution episodes in European cities. *Proc. Mixing Height and Inversions in Urban Areas, COST Action 715, EUR 20451,* Toulouse, France, European Commission, 65–74.

Steyn, D., S. Wekker, M. Kossmann, and A. Martilli, 2013: Boundary layers and air quality in mountainous terrain. *Mountain Weather Research and Forecasting,* F. K. Chow, S. F. J. De Wekker, and J. B. Snyder, Eds., Springer, 261–289.

Toro, M. V., J. J. Ramírez, R. A. Quiceno, and C. A. Zuluaga, 2001: Cálculo de la emisión vehicular de contaminantes atmosféricos en la ciudad de Medellín mediante factores de emisión Corinair. *Rev. Acodal,* **191,** 42–49.

Vergeiner, I., and E. Dreiseitl, 1987: Valley winds and slope winds—Observations and elementary thoughts. *Meteor. Atmos. Phys.,* **36,** 264–286, doi:10.1007/BF01045154.

Warner, T., 2011: *Numerical Weather and Climate Prediction*. Cambridge University Press, 526 pp.

Wesson, G., K. Gabriel, and L. Chun-Ta, 2001: Sensible heat flux estimation by flux variance and half-order time derivative methods. *Water Resour. Res.,* **37,** 2333–2343, doi:10.1029/2001WR900021.

Whiteman, C. D., 1982: Breakup of temperature inversions in deep mountain valleys: Part I. Observations. *J. Appl. Meteor.,* **21,** 270–289, doi:10.1175/1520-0450(1982)021<0270:BOTIID>2.0.CO;2.

——, 2000: *Mountain Meteorology: Fundamentals and Applications*. Oxford University Press, 376 pp.

——, and T. B. McKee, 1977: Observations of vertical atmospheric structure in a deep mountain valley. *Meteor. Atmos. Phys.,* **26,** 39–50.

——, and ——, 1982: Breakup of temperature inversions in deep mountain valleys: Part II. Thermodynamic model. *J. Appl. Meteor.,* **21,** 290–302, doi:10.1175/1520-0450(1982)021<0290:BOTIID>2.0.CO;2.

——, K. J. Allwine, L. J. Fritschen, M. M. Orgill, and J. R. Simpson, 1989: Deep valley radiation and surface energy budget microclimates. Part I: Radiation. *J. Appl. Meteor.,* **28,** 414–426, doi:10.1175/1520-0450(1989)028<0414:DVRASE>2.0.CO;2.

——, S. Eisenbach, B. Pospichal, and R. Steinacker, 2004: Comparison of vertical soundings and sidewall air temperature measurements in a small Alpine basin. *J. Appl. Meteor.,* **43,** 1635–1647, doi:10.1175/JAM2168.1.

Wilson, J. G., S. Kingham, J. Pearce, and A. P. Sturman, 2005: A review of intraurban variations in particulate air pollution: Implications for epidemiological research. *Atmos. Environ.,* **39,** 6444–6462, doi:10.1016/j.atmosenv.2005.07.030.

Yao, W., and S. Zhong, 2009: Nocturnal temperature inversions in a small, enclosed basin and their relationship to ambient atmospheric conditions. *Meteor. Atmos. Phys.,* **103,** 195–210, doi:10.1007/s00703-008-0341-4.

Zhong, S., C. Whiteman, and X. Bian, 2004: Diurnal evolution of three-dimensional wind and temperature structure in California's Central Valley. *J. Appl. Meteor.,* **43,** 1679–1699, doi:10.1175/JAM2154.1.

Zoumakis, N., and G. Efstathiou, 2006: Parameterization of inversion breakup in idealized valleys. Part II: Thermodynamic model. *J. Appl. Meteor. Climatol.,* **45,** 609–623, doi:10.1175/JAM2354.1.